Inorganic Chemistry

Article

pubs.acs.org/IC

Luminescent Gold and Silver Complexes with the Monophosphane 1-(PPh_2)-2-Me-$C_2B_{10}H_{10}$ and Their Conversion to Gold Micro- and Superstructured Materials

Olga Crespo,*[,†] Carlos Díaz,[‡] Colm O'Dwyer,[§,∥,⊥] M. Concepción Gimeno,*[,†] Antonio Laguna,[†] Isaura Ospino,[†] and Maria Luisa Valenzuela[#]

[†]Departamento de Química Inorgánica, Universidad de Zaragoza-CSIC, Instituto de Síntesis Química y Catálisis Homogénea (ISQCH), Pedro Cerbuna 12, 50009 Zaragoza, Spain

[‡]Departamento de Química, Facultad de Ciencias, Universidad de Chile, Las Palmeras 3425 Nuñoa, Casilla 653, Santiago, Chile

[§]Department of Chemistry, University College Cork, College Road, Cork, Ireland

[∥]Micro & Nanoelectronics Centre, Tyndall National Institute, Lee Maltings, Dyke Parade, Cork, Ireland

[⊥]Materials and Surface Science Institute, University of Limerick, Limerick, Ireland

[#]Dirección de Investigación y Postgrado, Universidad Autónoma de Chile, Av. Carlos Antúnez 1920, Santiago, Chile

ABSTRACT: Gold and silver complexes containing the monophosphane 1-PPh_2-2-Me-l,2-$C_2B_{10}H_{10}$ with different coordination numbers (2, 3) have been synthesized: [M(7,8-(PPh_2)$_2$-$C_2B_9H_{10}$)(1-PPh_2-2-Me-$C_2B_{10}H_{10}$)] (M = Ag, Au) and [Au_2(μ-1,n-$C_2B_{10}H_{10}$)(1-PPh_2-2-Me-$C_2B_{10}H_{10}$)$_2$] (n = 2, 12). Solid-state pyrolysis of [AuCl(1-PPh_2-2-Me-$C_2B_{10}H_{10}$)] and [Au_2(μ-1,12-$C_2B_{10}H_{10}$)(1-PPh_2-2-Me-$C_2B_{10}H_{10}$)$_2$] in air and of solutions of [AuCl(1-PPh_2-2-Me-$C_2B_{10}H_{10}$)] deposited on silicon and silica at 800 °C results in single-crystal Au, confirmed by diffraction and SEM-EDS. The morphology of the pyrolytic products depends on the thermolytic conditions, and different novel 3-D superstructures or microcrystals are possible. We also propose a mechanism for the thermal conversion of these precursors to structural crystalline and phase pure materials. The presence of the carborane monophosphane seems to originate quenching of the luminescence at room temperature in the complexes [Au_2(μ-1,n-$C_2B_{10}H_{10}$)(1-PPh_2-2-Me-$C_2B_{10}H_{10}$)$_2$], in comparison with other [Au_2(μ-1,n-$C_2B_{10}H_{10}$)L_2] species (L = monophosphane).

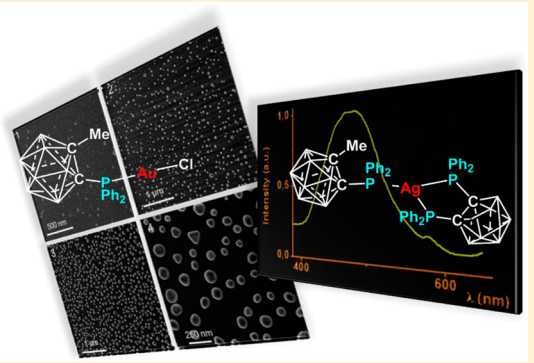

INTRODUCTION

The monophosphane 1-(PPh_2)-2-Me-$C_2B_{10}H_{10}$ has been selected for this work due to its electron-withdrawing capacity and chemical and thermal stability (both due to the skeleton based on the carborane cluster). The aim is to analyze the influence of this ligand in the products and structures resulting from the pyrolysis of gold complexes and in the luminescence properties of the complexes synthesized.

From a synthetic point of view we have taken into account the varieties of complexes reported with carborane monophosphanes.[1,2] They consist of mononuclear complexes of stoichiometry [AuClL] (L = (PCl^tBu)-$C_2B_{10}H_{11}$, 1-(PPh_2)-2-Ph-$C_2B_{10}H_{10}$, P(CH_2-1-$C_2B_{10}H_{11}$)$_3$) (Figure 1)[1] and [Au(7-(PPh_2)-8-R-$C_2B_9H_{10}$)(PPh_3)] (R = Me, Ph, SBz, SEt).[2a−c] Mixed gold−rhodium or gold−ruthenium metallocarborane complexes (Scheme 1)[2b] and the metallorhodium complex [Ag_2(thf)$_2$(OTf)$_2${1-(PPh_2)-3(η^5-Cp*)-3,1,2-$RhC_2B_{10}H_{10}$}$_2$] have also been synthesised, in which no Rh···Ag interactions are present and the two silver atoms are bridged by two triflate ligands.[2d] We have focused our attention on two- and three-coordinated gold and silver complexes.

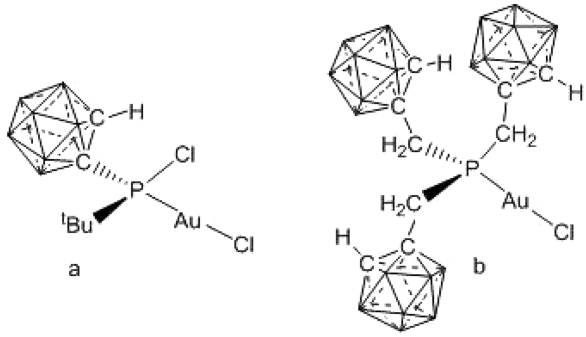

Figure 1. Gold complexes with carborane monophosphanes.

Received: March 11, 2014
Published: June 24, 2014

   dx.doi.org/10.1021/ic5005424 | *Inorg. Chem.* 2014, 53, 7260−7269

Scheme 1

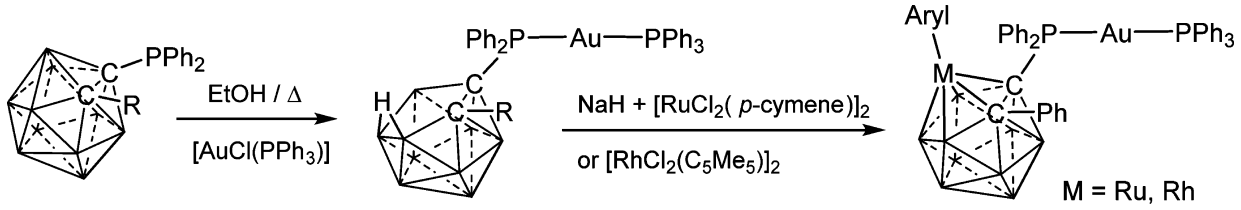

Organometallic derivatives have also been synthesized, taking into account that organometallic complexes with C-(carboranyl)−Au σ-bonds are well represented for the *ortho* isomer[3] but are almost unknown for the *meta* isomer.[4] Recently we reported the synthesis and crystal structure of the first example of such complexes with the *p*-carborane isomer.[3g]

The carborane cage in dicarba-*closo*-dodecaboranes displays high stability under many reaction conditions, which include oxidizing agents, alcohols, and strong acids. The thermal and thermo-oxidative stabilities of carborane-containing polymers are also interesting and useful properties. Pyrolysis of such polymeric materials has been previously described, and the salient features of the process have been established. The formation of ceramic materials (including C−Si−B) and micro- or nanoscale BPO_4 and $SiC/B_4C/C$ nanocomposites has been reported.[5] We have found that gold derivatives such as *gem*-$[N_3P_3(O_2C_{12}H_8)_2(OC_5H_4N\text{-}4\{Au(C_6F_5)\})_2]$ and its polymer $[\{NP(O_2C_{12}H_8)\}_{0.7}\{NP(OC_5H_4N\text{-}4\{Au(C_6F_5))_2\}_{0.3}]_n$ are useful precursors for nanostructured Au.[6] The pyrolysis of the carborane polyphosphazene $\{[NP(\{OCH_2\}_2C_2B_{10}H_{10})]_{0.5}[NP(\{OCH_2\}_2C_2B_9H_{10}\cdot NBu_4)]_{0.5}\}_n$ affords nanostructured BPO_4.[5d] We have also analyzed the deposition of micro- and nanoscale gold and silver structures after direct pyrolysis on silicon and silica surfaces.[7] Thus, we are interested in the resulting material and the final structures obtained upon pyrolysis of carborane derivatives with gold content.

Luminescence has been revealed as a property of several complexes and is useful in medicine both in diagnosis (for immunoassay) and in photodynamic therapy.[8] In addition, in the design of volatile organic compound (VOC) detectors, the presence of organic molecules may change the emission maxima or even lead to luminescence quenching. On the other hand, complexes with a triplet excited state may be used as phosphor dopants in the fabrication of phOLEDs (phosphorescent organic/organometallic light emitting diodes).[9] Taking into account these facts, the work has been completed with the analyses of the luminescent properties of the complexes synthesized, as dicarba-*closo*-dodecaboranes themselves and their derivatives, including different coordination complexes and the effect of the incorporation of fluorescent molecules in the carborane cage, have been reported.[3g,10] As part of our previous studies we have analyzed different mononuclear $[M(7\text{-}(PR_2)\text{-}8\text{-}Ph\text{-}C_2B_9H_{10})L]$[10s,t,v] (M = Au, Ag, Cu; L = monophosphane) and dinuclear $[Au_2(\mu\text{-}1,n\text{-}C_2B_{10}H_{10})(PR_3)_2]$ (n = 2, 7, 12)[3g] systems with carborane backbones. In this work we are interested in the effect of the electron-withdrawing carborane monophosphane 1-(PPh_2)-2-Me-$C_2B_{10}H_{10}$ on the luminescent properties of these systems.

Thus we present different gold and silver complexes with the 1-(PPh_2)-2-Me-$C_2B_{10}H_{10}$ monophosphane. Many of the properties of the carborane derivatives, some of which were mentioned above, are enhanced by increasing the boron content. Thus, in most cases, the synthesis has been directed to obtain molecules with high boron content. We also report the influence of the carborane monophosphane on the luminescent properties of mononuclear $[M(7,8\text{-}(PPh_2)_2\text{-}C_2B_9H_{10})(PR_3)]$ and dinuclear $[Au_2(\mu\text{-}1,n\text{-}C_2B_{10}H_{10})(PR_3)_2]$ (n = 2, 12) gold systems and the thermolysis of gold complexes containing carborane ligands, in order to elucidate if the resulting material will be nanostructured Au, BPO_4, or both, what its crystal structure will be, and whether or not the resulting material is a complex composite. To the authors' knowledge, this is the first dedicated investigation of pyrolysis into monomeric (not polymeric) carborane materials that includes the *para* isomer, as opposed to previous thermolytic studies using *o*-carborane derivatives. Thus, these complexes allow the evaluation of the effect of the nature of the carborane precursor, i.e. one gold atom by one carborane unit with two gold atoms by three carborane units, on the phase, morphology, and size of the pyrolytic products.

EXPERIMENTAL SECTION

General Comments. $[AuCl(tht)]$[11] (tht = SC_4H_8) and the monophosphane[12] 1-(PPh_2)-2-Me-$C_2B_{10}H_{10}$ were synthesized according to published procedures. Other reagents and solvents were used as received. When anhydrous solvents were needed, they were obtained from the solvent purification system (SPS) PS-MD-5 Innovative Technology, Scharlab. Solution ^1H and $^{31}P\{^1H\}$ NMR spectra were recorded using Bruker Avance 400 and Bruker ARX 300 spectrometers. The chemical shifts (δ) were referenced to $SiMe_4$ (^1H, external) or 85% H_3PO_4 (^{31}P, external). Steady-state photoluminescence spectra were recorded with a Jobin-Yvon Horiba Fluorolog FL-3-11 spectrometer.

[AuCl(1-PPh$_2$-2-Me-C$_2$B$_{10}$H$_{10}$)] (1). To a dichloromethane solution (15 mL) of 1-PPh_2-2-Me-$C_2B_{10}H_{10}$ (0.2 mmol, 68.5 mg) was added $[AuCl(tht)]$ (0.2 mmol, 64.1 mg). The mixture was stirred for 1 h, and then the solution was concentrated to ca. 3 mL under reduced pressure. Precipitation of **1**, as a white solid, was afforded by addition of *n*-hexane. Yield: 97%. Anal. Found: C, 31.31; H, 3.96. Calcd for $C_{15}H_{23}AuB_{10}ClP$: C, 31.34; H, 4.03. ^1H NMR ($CDCl_3$, ppm): 0−3 (m, br, 10H, BH), 2.39 (s, 3H, CH_3-Me), 7.61−7.69 (m, br, 5H, Ph), 8.17−8.23 (m, br, 5H, Ph). $^{31}P\{^1H\}$ NMR ($CDCl_3$, ppm): 50.9 (s). IR (cm^{-1}): ν(BH) 2570 (st), ν(AuCl) 327 (st).

[Au(1-PPh$_2$-2-Me-C$_2$B$_{10}$H$_{10}$)(tht)]OTf (2). A dichloromethane solution (15 mL) of 1-PPh_2-2-Me-$C_2B_{10}H_{10}$ (0.2 mmol, 68.5 mg) was added to a freshly prepared solution of $[Au(tht)_2]OTf$ (0.2 mmol) ($[Au(tht)_2]OTf$ was synthesized in situ from 0.2 mmol of $[AuCl(tht)]$ (64.1 mg), AgOTf (56.5 mg), and tht (17.63 μL) in dichloromethane). The mixture was stirred for 1.5 h and concentrated under reduced pressure. Compound **2**, as a white solid, was obtained by addition of *n*-hexane. Yield: 84%. Anal. Found: C, 30.44; H, 4.15; S, 8.73. Calcd for $C_{20}H_{31}AuB_{10}F_3O_3PS_2$: C, 30.93; H, 4.02; S, 8.26. ^1H NMR ($CDCl_3$, ppm): 0−3.5 (m, br, 10H, BH), 2.27−2.31 (m, br, 4H, CH_2-tht), 2.34 (s, 3H, CH_3-Me), 3.66 (m, br, 4H, CH_2-tht), 7.70 (br, 5H, Ph), 8.18−8.23 (m, br, 5H, Ph).$^{31}P\{^1H\}$ NMR ($CDCl_3$, ppm): 54.4 (s). ^{19}F NMR ($CDCl_3$, ppm): −78.1 (s, OTf). IR (cm^{-1}): ν(BH) 2578 (st), $\nu_{as}(SO_3)$ 1287 (st), $\nu_{sim}(CF_3)$ 1223 (st), $\nu_{as}(CF_3)$ 1162 (st), $\nu_{sim}(SO_3)$ 1025 (st).

[Au(1-PPh$_2$-2-Me-C$_2$B$_{10}$H$_{10}$)$_2$]OTf (3). *Method A.* A dichloromethane solution (20 mL) of 1-PPh_2-2-Me-$C_2B_{10}H_{10}$ (0.4 mmol,

dx.doi.org/10.1021/ic5005424 | Inorg. Chem. 2014, 53, 7260−7269

137.6 mg) was added to a freshly prepared solution of [Au(tht)$_2$]OTf (0.2 mmol) (synthesized in situ as described for complex **2**). The mixture was stirred for 2 h. The solution was then concentrated under reduced pressure, and the product, as a white solid, was obtained by addition of *n*-hexane.

Method B. To a dichloromethane solution (20 mL) of [Au(1-PPh$_2$-2-Me-C$_2$B$_{10}$H$_{10}$)(tht)]OTf (**2**; 0.2 mmol, 155.3 mg) was added 1-PPh$_2$-2-Me-C$_2$B$_{10}$H$_{10}$ (0.2 mmol, 68.5 mg). Then the procedure was similar to that described in method A. Yield: 78%. Anal. Found: C, 35.64; H, 4.11; S, 3.94. Calcd for $C_{31}H_{46}AuB_{20}F_3O_3P_2S$: C, 36.11; H, 4.49; S, 3.11. ^{1}H NMR (CDCl$_3$, ppm): 1−3 (m, br, 20H, BH), 2.15 (s, 6H, CH), 7.76 (br, 10H, Ph), 8.20 (br, 10H, Ph). ^{31}P{^{1}H} NMR (CDCl$_3$, ppm): 62.4 (s). ^{19}F NMR (CDCl$_3$, ppm): −78.3 (s, OTf). IR (cm^{-1}): ν(BH) 2586 (st), ν_{as}(SO$_3$) 1271 (st), ν_{sim}(CF$_3$) 1252 (st), ν_{as}(CF$_3$) 1156 (st), ν_{sim}(SO$_3$) 1028 (st).

[M(7,8-(PPh$_2$)$_2$-C$_2$B$_9$H$_{10}$)(1-PPh$_2$-2-Me-C$_2$B$_{10}$H$_{10}$)] (M = Ag (4), Au (5)). A solution (20 mL) of 1-PPh$_2$-2-Me-C$_2$B$_{10}$H$_{10}$ (0.2 mmol, 68.5 mg) in ethanol was added to a solution of [MX(1,2-(PPh$_2$)$_2$-C$_2$B$_{10}$H$_{10}$)] (0.2 mmol; MX = Ag(OTf) 153.9 mg, MX = AuCl 149 mg) in ethanol. The mixture was refluxed for 1.5 h and a white (**4**) or yellow (**5**) solid appeared, which was collected by filtration and washed with *n*-hexane. Data for **4** are as follows. Yield: 87%. Anal. Found: C, 51.53; H, 5.10. Calcd for $C_{41}H_{53}AgB_{19}P_3$: C, 51.72; H, 5.61. ^{1}H NMR (CDCl$_3$, ppm): −2.08 (s, br, 1H, B−H−B), 0−3 (m, br, 19H, BH), 1.90 (s, 3H, CH$_3$-Me), 6.92−7.24 (v.m, br, 10H, Ph), 7.30−7.64 (v.m, br, 15H, Ph), 7.90−7.94 (m, br, 5H, Ph). ^{31}P{^{1}H} NMR (300 MHz, CDCl$_3$, ppm): δ_A 40.9, δ_X 19.6; J[^{109}Ag−P$_A$] 583.4 Hz, J[^{109}Ag−P$_X$] 383.4 Hz, J_{AX} 63.4 Hz. IR (cm^{-1}): ν(BH) 2542 (st). Data for **5** are as follows. Yield: 87%. Anal. Found: C, 47.13; H, 5.10. Calcd for $C_{41}H_{53}AuB_{19}P_3$: C, 47.29; H, 5.13. ^{1}H NMR (CDCl$_3$, ppm): −2.12 (s, br, 1H, B−H−B), 0−3 (m, br, 19H, BH), 1.68 (s, 3H, CH), 7.15−7.22 (m, br, 4H, Ph), 7.30−7.46 (v m, br, 14H, Ph), 7.55−7.63 (m, br, 8H, Ph), 7.91−7.96 (m, br, 4H, Ph). ^{31}P{^{1}H} NMR (CDCl$_3$, ppm): AB$_2$ system δ_A 68.8, δ_B 60.0; J_{AB} = 138.1. IR (cm^{-1}): ν(BH) 2541 (st).

[Au(1-PPh$_2$-2-Me-C$_2$B$_{10}$H$_{10}$)(1,2-(PPh$_2$)$_2$-C$_2$B$_{10}$H$_{10}$)]OTf (6). A solution (20 mL) of [Au(1-PPh$_2$-2-Me-C$_2$B$_{10}$H$_{10}$)(tht)]OTf (**7**; 0.2 mmol, 155.3 mg) in dichloromethane was added to a solution of 1,2-(PPh$_2$)$_2$-C$_2$B$_{10}$H$_{10}$ (0.2 mmol, 102.4 mg) in dichloromethane. The mixture was stirred for 1.5 h. The solution was then concentrated to ca. 3 mL under reduced pressure, and the product, as a pale yellow solid, was obtained by addition of *n*-hexane. Yield: 75% (white). Anal. Found: C, 41.81; H, 4.51; S, 2.57. Calcd for $C_{62}H_{84}Au_2B_{30}F_6O_6P_4S_3$: C, 42.10; H, 4.20; S, 2.67. ^{1}H NMR (CDCl$_3$, ppm): 1−3.5 (m, br, 20H, BH), 2.29 (s, 3H, CH), 7.42−7.90 (v m, br, 25H, Ph), 8.16−8.21 (m, br, 5H, Ph). ^{31}P{^{1}H} NMR (CDCl$_3$, ppm): δ_A 70.9, δ_X 57.8; J_{AX} = 146.25 Hz ($\Delta\nu \gg J$). ^{19}F NMR (CDCl$_3$, ppm): −78.1 (s, OTf). IR (cm^{-1}): ν(BH) 2575 (st), ν_{as}(SO$_3$) 1272 (st), ν_{sim}(CF$_3$) 1222 (st), ν_{as}(CF$_3$) 1153 (st), ν_{sim}(SO$_3$) 1028 (st).

[Au(1-PPh$_2$-2-Me-C$_2$B$_{10}$H$_{10}$)(PPh$_3$)]OTf (7). A solution (20 mL) of [Au(1-PPh$_2$-2-Me-C$_2$B$_{10}$H$_{10}$)(tht)]OTf (**2**; 0.2 mmol, 155.3 mg) in dichloromethane was added to a solution of PPh$_3$ (0.2 mmol, 52.4 mg) in dichloromethane. The mixture was stirred for 1.5 h. The solution was then concentrated to ca. 3 mL under reduced pressure, and a white solid was obtained by addition of *n*-hexane. The solid contains a mixture of complex **7** and the homoleptic species [Au(1-PPh$_2$-2-Me-C$_2$B$_{10}$H$_{10}$)$_2$]OTf and [Au(PPh$_3$)$_2$]OTf. The following NMR data correspond to **7**. ^{1}H NMR (CDCl$_3$, ppm): 0.5−3 (m, br, 10H, BH), 2.27 (s, 3H, CH), 7.51−7.73 (v.m, br, 15H, Ph), 8.16−8.21 (m, br, 10H, Ph). ^{31}P{^{1}H} NMR (CDCl$_3$, ppm): AB system; δ_A 43.1(d, PPh$_3$), δ_B 61.1 (d, PPh$_2$), J_{AB} = 325.5 Hz. ^{19}F NMR (CDCl$_3$, ppm): −78.1 (s, OTf).

[Au$_2$(μ-1,*n*-C$_2$B$_{10}$H$_{10}$)(1-PPh$_2$-2-Me-C$_2$B$_{10}$H$_{10}$)$_2$] (*n* = 2 (8), 12 (9)). To a 0 °C diethyl ether solution (20 mL) of *o*- or *p*-carborane 1,*n*-(CH)$_2$B$_{10}$H$_{10}$ (*n* = 2, 12; 28.4 mg, 0.2 mmol), under an argon atmosphere, was added Li^{n}Bu (*n*-hexane solution 1.6 M, 0.38 mL, 0.6 mmol), and the mixture was stirred for 1.5 h (**8**) or 2.5 h (**9**). The solution was warmed to room temperature, and [AuCl(1-PPh$_2$-2-Me-C$_2$B$_{10}$H$_{10}$)] (0.35 mmol, 201 mg) was added. The suspension was stirred for 4.5 h (**8**) or 1.5 h (**9**) and the remaining solid filtered through Celite. The filtrate was concentrated under reduced pressure, and *n*-hexane was added to give a pale yellow solid, which was collected by filtration. Data for **8** are as follows. Yield: 87%. Anal. Found: C, 31.87; H, 4.89. Calcd for $C_{32}H_{56}Au_2B_{30}P_2$: C, 31.47; H, 4.62. ^{1}H NMR (CDCl$_3$, ppm): 1−3 (m, br, 30H, BH); 2.36 (s, 6H, CH$_3$-Me); 7.43−7.46 (m, br, 5H, Ph), 7.62 (m, br, 5H, Ph), 7.99−8.04 (m, br, 10H, Ph). ^{31}P{^{1}H} NMR (CDCl$_3$, ppm): 54.5 (s). IR (cm^{-1}): ν(BH) 2562 (st). Data for **9** are as follows. Yield: 87%. Anal. Found: C, 31.19; H, 4.18. Calcd for $C_{32}H_{56}Au_2B_{30}P_2$: C, 31.47; H, 4.62. ^{1}H NMR (CDCl$_3$, ppm): 1−3 (m, br, 30H, BH), 2.32 (s, 6H, CH), 7.55−7.63 (m, br, 12H, Ph), 8.04−8.10 (m, br, 8H, Ph). ^{31}P{^{1}H} NMR (CDCl$_3$, ppm): 53.4 (s). IR (cm^{-1}): ν(BH) 2580 (st).

Crystallography. Crystals were mounted in inert oil on glass fibers and transferred to the cold gas stream of a Xcalibur diffractometer equipped with a low-temperature attachment. Data were collected using monochromated Mo Kα radiation (λ = 0.71073 Å). Absorption corrections: SADABS.[13] The structures were refined on F^2 using the program SHELXL-97.[14] Selected details of the data collection and refinement are given in Table 1. CCDC 962746 and 962747 contain supplementary crystallographic data for complexes **5** and **8**, respectively, reported in this paper. These data can be obtained free of charge from the Cambridge Crystallographic Data Centre via www.ccdc.cam.ac.uk.data-request/cif.

Table 1. X-ray Data for Complexes 5 and 8

	5	8
formula	$C_{41}H_{53}AuB_{19}P_3$	$C_{34.5}H_{61}Au_2B_{30}Cl_5P_2$
cryst syst	triclinic	triclinic
space group	$P\bar{1}$	$P\bar{1}$
cell constant		
a (Å)	12.033(2)	12.631(3)
b (Å)	14.106(3)	13.741(3)
c (Å)	15.195(3)	18.619(4)
α (deg)	81.71(3)	95.48(3)
β (deg)	71.56(3)	106.80(3)
γ (deg)	73.15(3)	100.43(3)
V (Å^3)/Z	2337.9(8)/2	3004.8(10)/2
D_{exptl} (Mg m^{-3})	1.479	1.584
μ (mm^{-1})	3.282	5.181
F(000)	1036	1382
$2\theta_{max}$ (deg)	50	52
no. of rflns		
measd	32 377	165 111
indep	8202	10 531
transmission max−min	0.827−0.639	0.653−0.395
R_{int}	0.0425	0.0261
no. of restraints/params	18/641	244/655
S	1.109	1.080
R_w (F^2, all rflns)	0.1493	0.1051
R ($I > 2\sigma(I)$)	0.0588	0.0431
max $\Delta\rho$ (e Å^{-3})	5.744	2.907

Casting and Pyrolysis. The pyrolysis experiments were conducted by pouring a weighed portion (0.05−0.15 g) of the precursor **1** or **9** into aluminum oxide boats that were placed in a furnace (Daihan oven Model Wise Therm FHP-12) under a flow of air, heating from 25 °C to upper temperature limits of 300 °C and then to 800 °C, followed by annealing for 2−4 h at rates of 10 °C min^{-1} in each case.

A drop of CH_2Cl_2 solution containing the mixtures (solutions/suspensions in the range 1×10^{-3}−5×10^{-4} g/mL) of **1** was cast over either a silicon or oxidized silicon surface and the solvent was evaporated. The Si or SiO_2 wafer (with 400 mg of thermally grown oxide) was subsequently pyrolyzed at 800 °C using a predefined temperature program (Daihan oven Model FHP-12) where the polymer samples were heated at a rate of 10 °C min^{-1} from room

dx.doi.org/10.1021/ic5005424 | Inorg. Chem. 2014, 53, 7260−7269

Scheme 2. [a]

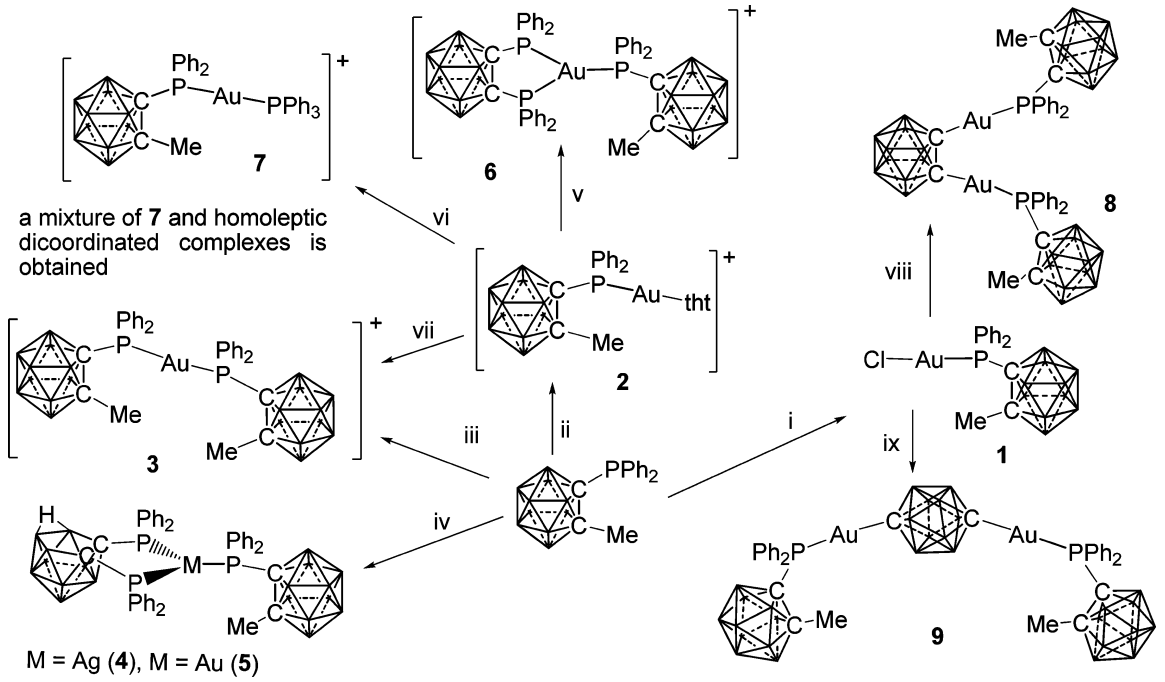

[a]Legend: (i) [AuCl(tht)], CH_2Cl_2; (ii) [$AuCl(tht)_2$]OTf, CH_2Cl_2; (iii) $^1/_2$[$AuCl(tht)_2$]OTf, CH_2Cl_2; (iv) [Ag(OTF)(1,2-$(PPh_2)_2$-$C_2B_{10}H_{10}$)] or [AuCl(1,2-$(PPh_{2)})_2$-$C_2B_{10}H_{10}$)], EtOH/Δ; (v) 1,2-$(PPh_2)_2$-$C_2B_{10}H_{10}$, CH_2Cl_2; (vi) PPh_3, CH_2Cl_2; (vii) 1-PPh_2-2-Me-$C_2B_{10}H_{10}$; (viii) 2Li^{n}Bu, *o*-carborane; (ix) 2Li^{n}Bu, *p*-carborane.

temperature to 800 °C under a constant air flow of 120 mL min^{-1} and subsequently annealed for 2 h. The resulting depositions give a uniform areal coverage for each mixture.

Electron Microscopy and Energy Dispersive X-ray Analysis. Scanning electron microscopy (SEM) and energy dispersive X-ray analysis (EDX) were carried out with a Hitachi S4800 and SU70 FESEM operating at 10 kV equipped with an Oxford Instruments X-max 50 mm^2 solid-state EDX detector for elemental line scanning and mapping. Suitably dispersed powders were also analyzed on holey carbon Cu grids by transmission electron microscopy (TEM) using a JEOL 2100F FEGTEM instrument operating at 200 kV.

RESULTS AND DISCUSSION

Synthesis and Characterization. Reaction of the monophosphane 1-PPh_2-2-Me-$C_2B_{10}H_{10}$ with [AuCl(tht)] or [Au-$(tht)_2$]$^+$ in a 1:1 molar ratio leads to the formation of [AuCl(1-PPh_2-2-Me-$C_2B_{10}H_{10}$)] (**1**) and [Au(1-PPh_2-2-Me-$C_2B_{10}H_{10}$)-(tht)]OTf (**2**), respectively. If the reaction with [$Au(tht)_2$]OTf is carried out in a 2:1 molar ratio, the compound [$Au(1\text{-}PPh_2\text{-}2\text{-}Me\text{-}C_2B_{10}H_{10})_2$]OTf (**3**) is obtained (Scheme 2).

In the IR spectra of complexes **1**−**3** the ν(BH) vibration appears between 2563 and 2606 cm^{-1}; in addition, the ν(Au−Cl) vibration appears in **1** and the absorptions attributed to the presence of the triflate anion in **2** and **3**. A broad signal from ca.1 to 3 ppm is assigned to the BH hydrogen atoms of the carborane moiety in the ^{1}H NMR spectra. The resonance corresponding to the methyl group of the carborane cage appears at about 2 ppm. Compound **2** also displays two multiplets due to the hydrogen atoms of the tht ligand. The three complexes display one singlet in the $^{31}P\{^1H\}$ NMR spectra between 50.9 and 62.4 ppm.

The three-coordinated complexes [Ag(7,8-$(PPh_2)_2$-$C_2B_9H_{10}$)(1-PPh_2-2-Me-$C_2B_{10}H_{10}$)] (**4**) and [Au(7,8-$(PPh_2)_2$-$C_2B_9H_{10}$)(1-PPh_2-2-Me-$C_2B_{10}H_{10}$)] (**5**), which contain a *closo*-carborane monophosphane and a *nido*-carborane diphosphane, may be obtained from the reaction of [Ag(OTf)(1,2-$(PPh_2)_2$-$C_2B_{10}H_{10}$)] or [AuCl(1,2-$(PPh_2)_2$-$C_2B_{10}H_{10}$)], with the monophosphane in refluxing ethanol (Scheme 1). During these reactions partial degradation of the carborane cluster of the diphosphane and coordination of the gold or silver center to the monophosphane takes place. The degradation of the carborane cage has been shown to be favored upon coordination of the diphosphane to a metallic center.[15] This idea could support the fact that it is the diphosphane and not the monophosphane which is partially degraded in the reaction. Nevertheless, we have carried out the reaction of the complex [AuCl(1-PPh_2-2-Me-$C_2B_{10}H_{10}$)] (**1**) with the diphosphane 1,2-$(PPh_2)_2$-$C_2B_{10}H_{10}$ in refluxing ethanol, and the result of the process is the formation of **5**. Thus, in both experiments it is the diphosphane which is partially degraded. Partial degradation of carborane clusters may take place with Lewis bases such as alkoxides, amines, fluorides, and even heterocyclic carbenes and consist of a nucleophilic attack of one of the two boron atoms nearest to the carbon atoms. In alcoholic media the RO^- groups are the nucleophilic species.[16] It has also been reported that coordination of the diphosphane to a metal enhances the partial degradation process.[17] A possible explanation for the selectivity for the partial degradation of the carborane cage belonging to the diphosphane over that of the monophosphane could be the presence of a PPh_2 group instead of a Me group, which would led to a more favorable nucleophilic attack over one of the boron atoms nearest to the carbon atoms.

The IR spectra and ^{1}H NMR spectra of compounds **4** and **5** prove the presence of the carborane clusters; in addition, the partial degradation of the carborane cages is confirmed by the presence of a broad signal at about −2 ppm in the ^{1}H NMR spectra, assigned to the bridging hydrogen atom in the open face of the *nido*-carborane. The $^{31}P\{^1H\}$ NMR spectra consist of AX_2 (**4**) or AB_2 (**5**) systems which confirm the expected

dx.doi.org/10.1021/ic5005424 | Inorg. Chem. 2014, 53, 7260−7269

geometry, but the pattern of that corresponding to **4** is complicated by coupling to the silver ^{107}Ag and ^{109}Ag nuclei.

The crystal structure of compound **5** has been elucidated by X-ray diffraction studies (Figure 2). The gold atom displays a

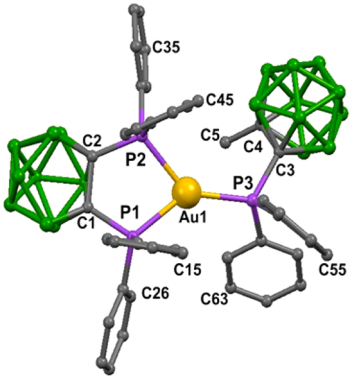

Figure 2. ORTEP representation of compound **5**. Hydrogen atoms have been omitted for clarity.

trigonal-planar geometry with the gold center 0.12 Å out of the plane formed by the three phosphorus atoms P1, P2, and P3. The major distortion is due to the chelate angle of the diphosphane (P−Au−P = 83.18(6)°).

The bond distances and angles may be compared (Table 2) with those of different three-coordinated species[18,5s,5t,5v] such as [Au(1,2-(PPh$_2$)$_2$-C$_2$B$_{10}$H$_{10}$)(PPh$_3$)]OTf and [Au(7,8-(PPh$_2$)$_2$-C$_2$B$_9$H$_{10}$)}(PR$_3$)] (PR$_3$ = monophosphane).

Complexes **1** and **2** contain a chloride and tht ligand, respectively, which, upon reaction with carbanionic species (as RLi) of the former or through substitution of the tht ligand in the latter, may lead to organometallic or metallorganic gold complexes (Scheme 1). Thus, substitution of tht in **2** by 1,2-(PPh$_2$)$_2$-C$_2$B$_{10}$H$_{10}$ leads to the formation of [Au(1-PPh$_2$-2-Me-C$_2$B$_{10}$H$_{10}$)(1,2-(PPh$_2$)$_2$-C$_2$B$_{10}$H$_{10}$)]OTf (**6**), which is analogous to **5** but contains two *closo*-carborane ligands and thus is an ionic compound. Similar features are observed in the IR and NMR spectra of **5** and **6**, except for the absence of the signal at −2 ppm and the presence of vibrations corresponding to the presence of the triflate group in the ^{1}H NMR and IR spectra of **6**, respectively. The ^{31}P{^{1}H} NMR spectrum of **6** consists of a AX$_2$ system.

The ^{31}P{^{1}H} NMR spectrum of the reaction of **2** with PPh$_3$ consists of a AB system assigned to the expected complex **7** and two singlets at 62.4 and 45.1 ppm corresponding to the homoleptic species [Au(1-PPh$_2$-2-Me-C$_2$B$_{10}$H$_{10}$)$_2$]OTf and [Au(PPh$_3$)$_2$]OTf, respectively. The equilibrium P^A−Au−P^B ↔ P^A−Au−P^A + P^B−Au−P^B in solution between mixed and homoleptic species is well-known in gold chemistry.[19]

As discussed above, the complex [AuCl(1-PPh$_2$-2-Me-C$_2$B$_{10}$H$_{10}$)] (**1**) may react with carbanionic reagents as RLi. Such processes afford the complexes [AuR(1-PPh$_2$-2-Me-C$_2$B$_{10}$H$_{10}$)]. We have chosen the *meta* and *para* isomers of carborane as R fragments. Thus, reaction of 1,*n*-(LiC)$_2$B$_{10}$H$_{10}$ (*n* = 2, 12) with **1** in the molar ratio 1:2 affords the organometallic complexes [Au$_2$(*μ*-1,*n*-C$_2$B$_{10}$H$_{10}$)(1-PPh$_2$-2-Me-C$_2$B$_{10}$H$_{10}$)$_2$] (**8**, *n* = 2; **9**, *n* = 12). The IR and ^{1}H NMR spectra confirm the presence of the carborane cluster. The ^{31}P{^{1}H} NMR spectra of both complexes display one singlet at about 54 ppm. The crystal structure of **8** has been elucidated by X-ray diffraction studies (Figure 3). The gold centers display a linear

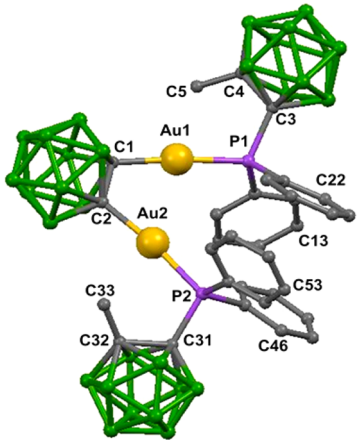

Figure 3. ORTEP representation of compound **8**. Hydrogen atoms have been omitted for clarity.

geometry. Gold distances and angles are in the range found for the complexes [Au$_2$(*μ*-1,*n*-C$_2$B$_{10}$H$_{10}$)(PPh$_3$)$_2$] (*n* = 2, 7, 12; PR$_3$ = PPh$_3$, PMe$_3$), which are shown in Table 3. No aurophilic contact has been found in **8** between the gold centers (Au···Au distance ca. 3.5 Å). Comparison of the Au−Au distances in Table 3 indicates that complexes with PPh$_3$ or PMe$_3$ display no aurophillic interaction. Therefore, the use of the smaller PMe$_3$ monophosphane seems not to lead to the presence of an aurophilic interaction. Aurophilic interactions have been found in complexes with diphosphane [7,8-(PPh$_2$)$_2$-C$_2$B$_9$H$_{10}$]$^-$ and dithiolate [1,2-S$_2$-C$_2$B$_{10}$H$_{10}$]$^{2-}$ carborane ligands.[20] Therefore, perhaps it is the carborane geometry that leads to such an orientation of the C−Au bonds that does not allow the two gold atoms to get closer to each other.

Luminescence Studies. The emission spectra of complexes **4** and **5** in the solid state at 298 K (Figure 4 and Table 4) exhibit one emission whose maximum appears at 397 nm (**4**) and at 480 nm (**5**). At 77 K, compound **4** shows one band with a maximum at 450 nm. Two different emissions are

Table 2. Bond Lengths and Angles for [Au(7,8-(PPh$_2$)$_2$-C$_2$B$_9$H$_{10}$)(1-PPh$_2$-2-Me-C$_2$B$_{10}$H$_{10}$)] (5) and Other Three-Coordinated Gold Complexes with Diphosphanecarborane Ligands

compd	P−Au−P (deg)[a]	Au−P$_3$ (Å)[b]	Au−P (Å)[a]	Au−P (Å)[c]
5	83.18(6)	0.12	2.4223(18), 2.4223(18)	2.3234(19)
[Au(dppnc)(PPh$_3$)][18b]	84.91(4)	0.07	2.3896(13), 2.3952(12)	2.2831(13)
[Au(dipnc)(PPh$_3$)][10s]	90.38(2)	0.15	2.4083(6), 2.3076(6)	2.3791(6)
[Au(dppc)(PPh$_3$)]ClO$_4$[18a]	90.2(1)	0.18	2.405(1), 2.417(1)	2.318(1)
[Au(dppnc)(PPh$_2$OEt)][10v]	83.15(6)	0.14	2.3917(19), 2.3934(18)	2.2579(19)

closo- and *nido*-carborane diphosphane: dppc, *closo*, R = Ph; dppnc, *nido*, R = Ph; dipnc, *nido*, R = ^{i}Pr. [a]Diphosphane. [b]Distance of the Au atom to the plane defined by the three phosphorus atoms. [c]Monophosphane.

dx.doi.org/10.1021/ic5005424 | Inorg. Chem. 2014, 53, 7260−7269

Table 3. Bond Lengths and Angles for 8 and Other Three-Coordinated Gold Complexes with Phosphanecarborane Ligands

	$[Au_2(\mu\text{-}1,n\text{-}C_2B_{10}H_{10})(PPh_3)_2]$			$[Au_2(\mu\text{-}1,2\text{-}C_2B_{10}H_{10})L_2]$	
distance (Å)/angle (deg)	$n = 2$[3f]	$n = 7$[4]	$n = 12$[3g]	L = PMe_3[3f]	L = 1-PPh_2-2-Me-$C_2B_{10}H_{10}$ (**8**)
C–C[a]	1.71(2)			1.693(5)	1.681(9)
C–Au	2.055(14), 2.033(15)	2.054(7), 2.047(7)	2.058(4)	2.049(4), 2.068(4)	2.047(6), 2.052(7)
Au–P	2.270(4), 2.273(5)	2.265(2), 2.271(2)	2.273(10)	2.262(12), 2.273(10)	2.2721(17), 2.2821(18)
Au···Au	3.567(1)	6.14		3.522(7)	3.516(1)
C–Au–P	178.9(4), 174.2(4)	179.3(2), 174.1(2)	175.7(10)	175.8(11), 175.7(10)	175.59(18), 173.14(18)

[a]Carborane carbon atoms.

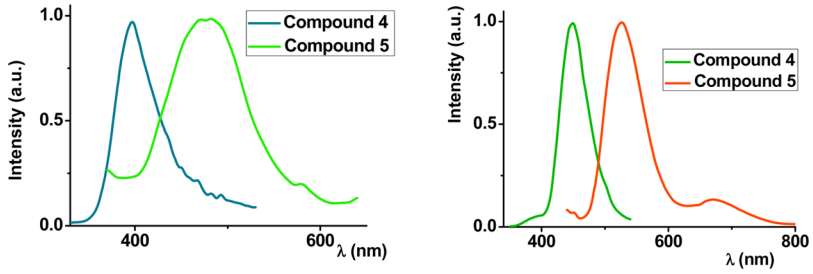

Figure 4. Normalized emission spectra of **4** and **5** at room temperature (left) and 77 K (right).

Table 4. Emission Maxima (nm) for Solid Samples of Complexes $[M(7,8\text{-}(PR_2)_2C_2B_xH_{10})\}(PR'_3)]^n$ ($x = 9$, $n = 0$; $x = 10$, $n = +1$; M = Au, Ag)

	λ_M	
compd	298 K	77 K
$[Ag(7,8\text{-}(PPh_2)_2\text{-}C_2B_9H_{10})(1\text{-}PPh_2\text{-}2\text{-}Me\text{-}C_2B_9H_{10})]$ (**4**)	397	450
$[Au(7,8\text{-}(PPh_2)_2\text{-}C_2B_9H_{10})(1\text{-}PPh_2\text{-}2\text{-}Me\text{-}C_2B_9H_{10})]$ (**5**)	480	526
		670
$[Au(7,8\text{-}(PPh_2)_2\text{-}C_2B_9H_{10})(PPh_3)]$[10s]	540	529
	670	676
$[Ag(7,8\text{-}(PPh_2)_2\text{-}C_2B_9H_{10})(PPh_3)]$[10v]	470	465
	500	515
$[Au(7,8\text{-}(PPh_2)_2\text{-}C_2B_9H_{10})(PPh_2(CH_2)_2Py)]$[10v]	510	520
		670
$[Ag(7,8\text{-}(PPh_2)_2\text{-}C_2B_9H_{10})(PPh_2(CH_2)_2Py)]$[10v]	530	500
$[Au(7,8\text{-}(PPh_2)_2\text{-}C_2B_9H_{10})(PPh_2OEt)]$[10v]	519	525
	670	670
$[Ag(7,8\text{-}(PPh_2)_2\text{-}C_2B_9H_{10})(PPh_2OEt)]$[10v]	400	398

observed for **5** at 77 K. Upon excitation at 320 nm the emission maximum appears at 526 nm. Excitation at lower energies leads to a weaker emission in the red region.

Our previous results indicate that the free *nido*-diphosphane and three-coordinated gold complexes $[M(7,8\text{-}(PR_2)_2C_2B_9H_{10})\}(PR'_3)]$ (M = Au, Ag, Cu; R = Ph, ^{i}Pr) are luminescent[10s−v] with lifetimes in the microsecond range[10t,v] and aid in the assignation of the origin of the emissions.

The emission observed in the blue-yellow region resembles that of the free *nido*-diphosphane. It has been assigned to intraligand transitions (IL) modified upon coordination to the metal. The energy maximum for this IL band is lower for the gold complex (**5**) in comparison with the silver complex (**4**). There is a shift to the red region upon coordination of the free diphosphane, in comparison with the emission of the free *nido*-diphosphane, and this shift follows the same trend reported for complexes $[M(7,8\text{-}(PR_2)_2C_2B_9H_{10})\}(PR'_3)]$ with other monophosphanes, for which the influence of the metal in this IL band follows the pattern Au > Ag. The red emission observed for **5** at 77 K is also consistent with the low-energy emissions observed for three-coordinate gold complexes with this diphosphane, which have been assigned to metal to ligand charge transfer (MLCT) transitions or a mixture of MLCT and intraligand charge transfer (ILCT) transitions.

We have also studied the luminescent characteristics of **8** and **9**, as different *ortho*, *meta*, and *para* dinuclear gold derivatives of stoichiometry $[Au_2(\mu\text{-}1,n\text{-}C_2B_{10}H_{10})(PR_3)_2]$ ($n = 2, 7, 12$; $PR_3 = PPh_3$, PMe_3) are luminescent (Figure 5 and Table 5).[3g] We

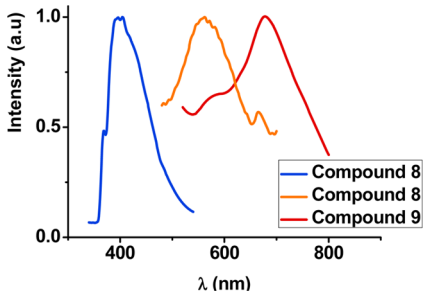

Figure 5. Normalized emission spectra of **8** (dual emission) and **9** at 77 K.

have found that **8** and **9** are not emissive in the solid state at room temperature. At 77 K, in the solid state, complex **8**

Table 5. Emission Maxima (nm) of Organometallic Gold Complexes with Carborane Ligands[a]

complex	room temp	77 K
$[Au_2(\mu\text{-}1,2\text{-}C_2B_{10}H_{10})(PPh_3)_2]$[3g]	368, 500	500, 570
$[Au_2(\mu\text{-}1,7\text{-}C_2B_{10}H_{10})(PPh_3)_2]$[3g]	364, 530	396, 510
$[Au_2(\mu\text{-}1,12\text{-}C_2B_{10}H_{10})(PPh_3)_2]$[3g]	350, 506	396, 555
$[Au_2(\mu\text{-}1,12\text{-}C_2B_{10}H_{10})(1\text{-}PPh_2\text{-}2\text{-}Me\text{-}C_2B_{10}H_{10})_2]$ (**9**)		680
$[Au_2(\mu\text{-}1,2\text{-}C_2B_{10}H_{10})(PMe_3)_2]$[3g]	391, 500	403, 516
$[Au_2(\mu\text{-}1,2\text{-}C_2B_{10}H_{10})(1\text{-}PPh_2\text{-}2\text{-}Me\text{-}C_2B_{10}H_{10})_2]$ (**8**)		410, 580

[a]The excitation wavelength is about 290 nm for the higher energy band and about 400 nm for the lower energy band.

dx.doi.org/10.1021/ic5005424 | Inorg. Chem. 2014, 53, 7260−7269

displays two bands. Upon excitation at 280 nm, an emission at 480 nm is observed, whereas excitation at lower energies leads to a band centered at 580 nm. Compound **9** displays one band at 680 nm upon excitation at 360 nm. Dual emission, at similar energies, has been observed for organometallic dinuclear complexes of the formula $[Au_2(\mu\text{-}1,n\text{-}C_2B_{10}H_{10})(PR_3)_2]$ (Table 5). The band at higher energy has been attributed to IL(carborane) transitions whose Stokes shift points to a fluorescent nature, and the band at lower energy is ascribed to charge transfer transitions involving the gold centers in the reported examples whose Stokes shift seems to point to a phosphorescent nature.

It is noticeable that **8** and **9,** both containing the carborane monophosphane, are not emissive at room temperature. Quenching processes are difficult to predict. Objective facts on comparison of $[Au_2(\mu\text{-}1,2\text{-}C_2B_{10}H_{10})(PPh_3)_2]$ and **8** are the more electron withdrawing nature of the carborane cluster, in comparison with the phenyl unit and the three-dimensional aromatic nature of the carborane cluster. Although a concrete quenching mechanism is difficult to predict, it is possible to discuss the different behaviors of **8** and **9** at room temperature and 77 K and the quenching of the IL emission at 77 K in **8** but not in **9** as follows: the rigidity imposed at 77 K could explain the emissive behavior at this temperature, as quenching processes are in many cases less favorable at low temperatures and rigidity favors the emissive behavior. Nevertheless, it is interesting to observe that the emission which is quenched in **9** at both room temperature and 77 K is that assigned to an IL (carborane) transition but not that at lower energy, attributed to charge transfer processes involving the gold center. It seems that for **9** at high temperature quenching of the first excited singlet occurs. When the temperature is lowered, intersystem crossing is more favorable than direct decay to the ground state and phosphorescent charge transfer transitions lead to red emission. Changing the *para* isomer in **9** to the *ortho* isomer in **8** seems to make intersystem crossing less favorable and thus both fluorescence and phosphorescence are observed in **8**.

Pyrolysis and Conversion to Gold Crystals. Two complexes have been selected for these studies, compound **1** (mononuclear) with 34.4% of gold and 18.8% boron content and compound **9** (dinuclear) with lower gold (32.3%) but higher boron (26.6%) content. Compounds **1** and **9** have been heated to 800 °C in air, whereas **1** was selected for the study after its deposition on Si or SiO_2 surfaces and dryness and heating to 800 °C.

Pyrolysis of $[AuCl(1\text{-}PPh_2\text{-}2\text{-}Me\text{-}C_2B_{10}H_{10})]$ *(**1**) and* $[Au_2(\mu\text{-}1,n\text{-}C_2B_{10}H_{10})(1\text{-}PPh_2\text{-}2\text{-}Me\text{-}C_2B_{10}H_{10})_2]$ *(**9**).* Pyrolysis of the Au precursors **1** and **9** at 800 °C in air results in a reddish yellow solid that adheres well to the crucible. XRD patterns indicate the presence of pure cubic gold crystals. The typical strong reflections for the (111), (200), (220), and (311) planes of metallic gold in a face-centerd cubic lattice were observed as shown in Figure 6,[10] for the pyrolytic product from **1**. A similar XRD pattern was observed for the product from thermolysis of **9**. SEM imaging shows, for both pyrolytic products, a spongelike porous morphology.[21] EDS analysis also confirmed that only pure Au is present. Consistent with the SEM observations, TEM analysis confirms the porous gold comprises agglomerated crystals arranged in a random matrix akin to a 3D disordered gyroidal morphology. Porous metals have been recently employed for ultrasensitive surface-enhanced Raman scattering (SERS) substrates[22] and have unique properties such as low density, gas permeability, and high surface area of high

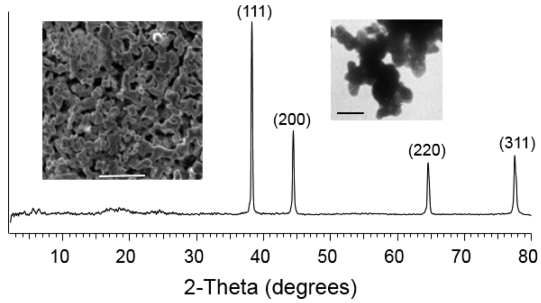

Figure 6. XRD patterns of crystalline porous Au from direct pyrolysis of compound **1**. Inset left: SEM image of the porous gold morphology (scale bar 5 μm). Inset right: TEM image of agglomerated crystals of the structure of the porous gold (scale bar 1.5 μm).

index crystal facets for catalysis, hydrogen storage, and other applications. Preparative methods for metal foams to date most commonly involve dealloying of bimetallic Au_xAg_y.[23]

Pyrolysis of $[AuCl(1\text{-}PPh_2\text{-}2\text{-}Me\text{-}C_2B_{10}H_{10})]$ *(**1**) Deposited on Silicon or Silica.* Using precursor **1**, we successfully afforded complex geometrically shaped single Au crystals directly from pyrolysis of the previously deposited sample. The important gold content in **1** (36.21%) leads to demixed phases and mobile agglomeration. This demixing process results from the interaction of inert Au NPs within a decomposing organic phase that undergoes carbonization. Prior to solidification as a carbon, the separated Au NPs migrate and agglomerate to crystallize as larger single crystals. This association process is similarly found in Au NPs on PMMA or PS thin films[24] and has been described by Avrami kinetics for solid species within liquid polymer films and by Ostwald ripening in thermally driven solid-state processes. In the present case, agglomeration and growth of a larger single crystal from the nanoparticles is observed to occur until the surrounding carbonaceous material solidifies. This solidification is the reason for the variety in sizes and geometries of the resulting crystals; their shape, dispersion, and size depend on the local density of building block NPs of Au formed through the initial decomposition of the gold-containing complexes.

The initially formed gold nanoparticulate clusters ripen to microcrystals with defined shapes. The growth of gold microcrystals eventually stops when triangular plates are formed. In some cases these plates ripen to full tetrahedra. This happens in some cases when sufficient gold source is present in the surrounding area (depending on the density of other growing crystals in the vicinity using the Au source within the deposit). Structural variants related to the cubic structure are mainly represented, followed by octahedral, fully formed crystals.

The gold comes from the complex, and the decomposing carborane precursor results in a carbon residue that is removed after the end of the pyrolytic process. Figure 7 illustrates this process.

Deposition on Si and pyrolysis (Figure 7a) lead to spherical crystals which develop faceting only if enough atomic source is available. As a high density of nucleated crystals is formed, many remain nonfaceted. At the earlier stages of the pyrolysis of the dichloromethane solutions of **1** deposited on silica (Figure 7b1), the crystals are found on the surface of a roughening carbon residue and subsequent time allows for shape development and diameter increase (Figure 7b2−b4).

dx.doi.org/10.1021/ic5005424 | *Inorg. Chem.* 2014, 53, 7260−7269

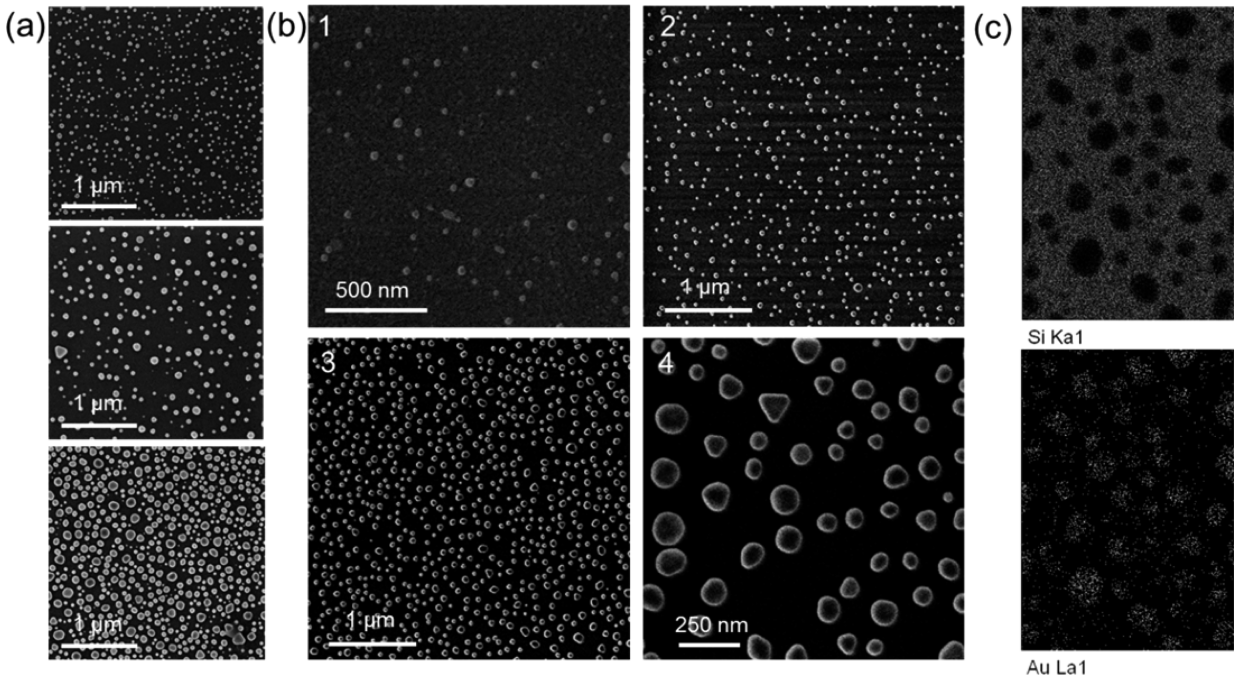

Figure 7. Various stages of the crystal growth where small low-density crystals eventually become a higher density of larger crystals with further pyrolysis followed by SEM images of precursor **1** deposited on Si (a) and SiO_2 (b1−b4) after pyrolysis. (c) EDX mapping confirming Au content for the particles and some regions of the surrounding precursor where the Au source has not agglomerated to the growing crystals.

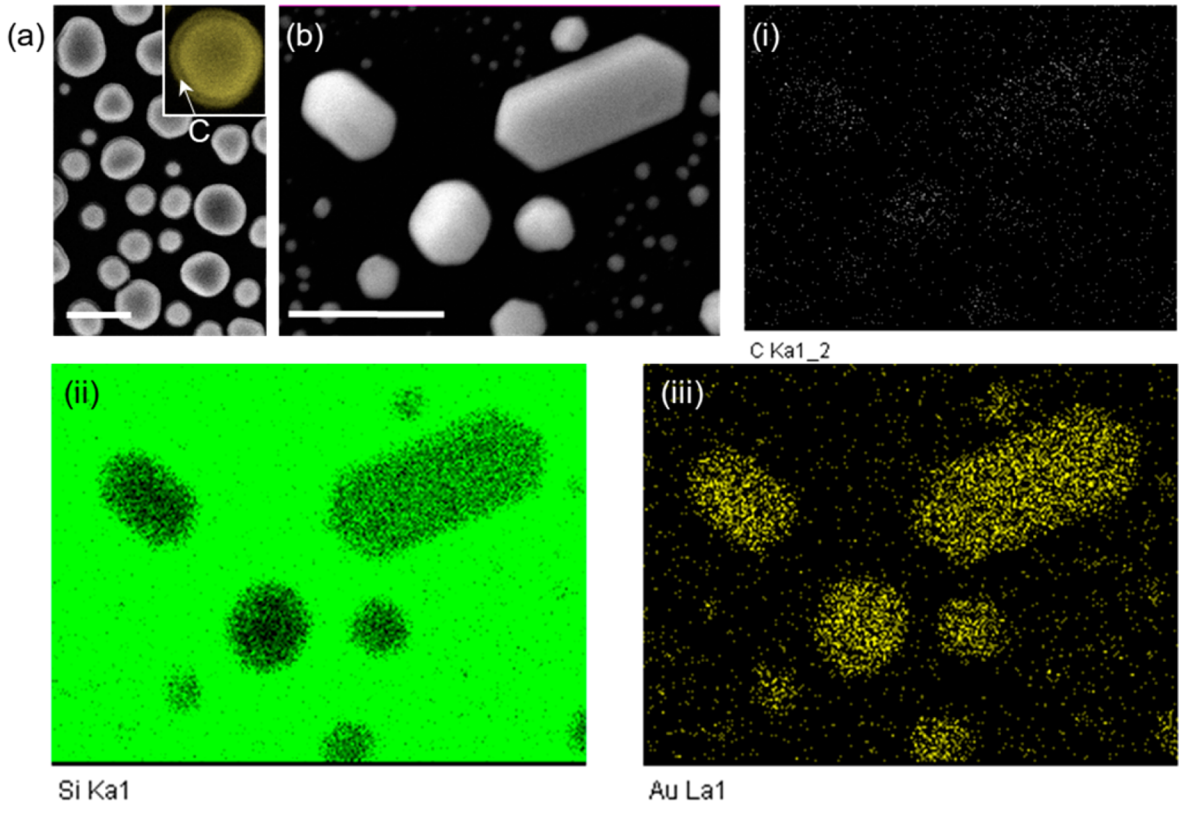

Figure 8. Studies of the pyrolysis of solutions in dichloromethane of **1** deposited on SiO_2: (a) early-stage Au crystal prior to full facet development coated with a remnant carbon overlayer (see inset; scale bar 100 nm); (b) EDS map analysis of elemental (i) C (white), (ii) Si substrate, and (ii) Au (yellow) (scale bar 1 μm).

Without reliance on ligands or shape selective surfactants (the organic matrix decomposes and thus does not fulfill this function in the present case) a random but uniform surface coverage of individual crystals (Figure 7a,b) shows the variety of crystal shapes possible through coarsening of NPs formed by cleavage, agglomeration, and ripening of metal atoms. Compositional analysis using EDX mapping in Figure 7c confirms that the polyhedral crystals are phase pure.

dx.doi.org/10.1021/ic5005424 | *Inorg. Chem.* 2014, 53, 7260−7269

Figure 8 shows that the early-stage crystals formed by pyrolysis of dichloromethane solutions of **1** deposited on SiO_2 are surrounded by a thin carbon coating. Larger crystals that are faceted also are likely to contain a very thin layer, and quantitative EDS shows that some remnant carbon is likely to stem from underlying carbon as the measurement also detects oxygen from the underlying substrate. Typically, the fully formed crystals post-pyrolysis are free from carbon coatings.

In terms of their formation, phase separation of the metal from the organic portion of the precursor is expected, as has been found in asymmetric polymer−particle mixtures[25] for large particle-to-monomer size ratios. An entropically driven surface phase transition has been observed[26] for low-M_w simpler polymer−particle thin films, resulting in the expulsion and layering of NPs along the solid substrate. Au association, observed in the bulk above a threshold temperature,[27] forms into a ripening phase that is bound to the surface and fed from the Au content within the surrounding matrix, within and on a carbonaceous material during pyrolysis. Low-M_w thin composite films have been shown to form a diffuse layer of NPs at the substrate interface after spin coating which failed to be redispersed by subsequent thermal annealing. A phase separation and crystallization, where NPs form due to the chemical decomposition, allows crystals to eventually grow due to the physical decomposition. The decomposition follows expected pathways, including carbonization and release of Au metals, similar to what we demonstrated using other forms of Au-containing phosphazene structures. There is no formal relationship between the nanostructures and the crystal structure of the compound. The nanostructures form from migration and crystallization of nanoparticles that are formed from the release of metal centers during decomposition, which is outlined in the paper. Further work will be required to determine the kinetics and coarsening/crystallization of metal crystals from these types of precursors.

CONCLUSIONS

Gold and silver complexes have been synthesized with the 1-PPh_2-2-Me-$C_2B_{10}H_{10}$ monophosphane. The complexes [AuCl(1-PPh_2-2-Me-$C_2B_{10}H_{10}$)] (**1**) and [Au(1-PPh_2-2-Me-$C_2B_{10}H_{10}$)(tht)]OTf (**2**) are good starting products in the synthesis of metalloorganic or organometallic derivatives.

The complexes [M(7,8-$(PPh_2)_2$-$C_2B_9H_{10}$)(1-PPh_2-2-Me-$C_2B_{10}H_{10}$)] (M = Ag (**4**), Au (**5**)) and [Au_2(μ-1,*n*-$C_2B_{10}H_{10}$)(1-PPh_2-2-Me-$C_2B_{10}H_{10}$)$_2$] (*n* = 1 (**8**), 12 (**9**)) are luminescent. Dual emission has been observed for **5** and **8**. The emissive behavior is attributed to the metal center and the *nido*-carborane diphosphane in the three-coordinated compounds or to the carborane cluster and the gold centers in the dinuclear complexes. The derivatives [M(7,8-$(PPh_2)_2$-$C_2B_9H_{10}$)(1-PPh_2-2-Me-$C_2B_{10}H_{10}$)] (M = Ag (**4**), Au (**5**)) follow the pattern observed for similar complexes with other monophosphanes. The influence of the metal in the emission energy of the band at higher energy follows the order Au > Ag. The complexes [Au_2(μ-1,*n*-$C_2B_{10}H_{10}$)(1-PPh_2-2-Me-$C_2B_{10}H_{10}$)$_2$] (*n* = 1 (**8**), 12 (**9**)) exhibit differences from homologues containing other monophosphanes. They are not luminescent at room temperature, and for compound **9** only the emission at lower energy is observed. Dual emissions have been observed for **8** at 77 K which are observed for analogous complexes with other monophosphanes at both room temperature and 77 K. The presence of the electron-withdrawing *closo*-carborane monophosphane leads to the quenching of both emissions at room temperature for **8** and **9** and to the emission at higher energy for **9** at 77 K. It seems that in **9** intersystem crossing is the most important process, leading only to the phosphorescent emission.

Compounds **1** and **9** are useful solid-state precursors for forming porous metals via agglomeration (but of individual single crystals) or shaped Au microcrystals depending on the pyrolysis conditions. As observed for other metals (noble and transition),[11,19,28] pyrolysis on Si or SiO_2 wafers produces crystals that include nanoparticle formation, mobility through the composite, and ripening crystallization into defined shapes with a relatively uniform spatial distribution when pyrolyzed on substrates. The decomposition process and resulting mechanism is inherently linked to the structure of the compounds. The use of molecular Au carborane monophosphane precursors leads to the formation of Au phase pure products, and the formation of BPO_4, which is a product of the pyrolysis of $\{[NP(\{OCH_2\}_2C_2B_{10}H_{10})]_{0.5}[NP(\{OCH_2\}_2C_2B_9H_{10}\cdot NBu_4)]_{0.5}\}_n$, has not been detected.

AUTHOR INFORMATION

Corresponding Authors

*E-mail for O.C.: ocrespo@unizar.es.

*E-mail for M.C.G.: gimeno@unizar.es.

Notes

The authors declare no competing financial interest.

ACKNOWLEDGMENTS

We thank the Ministerio de Economía y Competitividad-FEDER (No. CTQ2010-20500-C02-01) and DGA-FSE (E77) and FONDECYT project 1120179. C.O. acknowledges support from a Science Foundation Ireland Award under contract no. 07/SK/B1232a and through the UCC Strategic Research Fund. Part of this work was conducted under the framework of the INSPIRE programme, funded by the Irish Government's Programme for Research in Third Level Institutions, Cycle 4, National Development Plan 2007−2013.

REFERENCES

(1) (a) Sterzik, A.; Rys, E.; Blaurock, S.; Hey-Hawkins, E. *Polyhedron* **2001**, *20*, 3007. (b) McWhannell, M. A.; Rosair, G. M.; Welch, A. J. *Acta Crystallogr., Sect. C* **1998**, *C54*, 13−15.

(2) (a) Crespo, O.; Gimeno, M. C.; Jones, P. G.; Laguna, A. *Acta Crystallogr. Sect. C* **2000**, *C56*, 46−47. (b) Teixidor, F.; Benakki, R.; Viñas, C.; Kivekäs, R.; Sillanpää, R. *Inorg. Chem.* **1999**, *38*, 5916−5919. (c) McWhannell, M. A.; Rosair, G. M.; Welch, A. J.; Teixidor, F.; Viñas, C. *J. Organomet. Chem.* **1999**, *573*, 165−170. (d) Huo, X.-K.; Su, G.; Jin, G.-X. *Chem. Eur. J.* **2010**, *16*, 12017−12027.

(3) (a) Mitchel, C. M.; Stone, F. G. A. *J. Chem. Soc. D* **1970**, 1263−1264. (b) Reid, B. D.; Welch, A. J. *J. Organomet. Chem.* **1992**, *438*, 371−384. (c) Crespo, O.; Gimeno, M. C.; Laguna, A.; Peña, A. M. *Polyhedron* **1998**, *17*, 4163−4167. (d) Baukova, T. V.; Kuzmina, L. G.; Dvortsova, N. V.; Porai-Koshits, M. A.; Kravtsov, D. N.; Perevalova, E. G. *Metalloorg. Khim.* **1989**, *2*, 1098−1105. (e) Batsanov, A. S.; Fox, M. A.; Hibbert, T. G.; Howard, J. A. K.; Kivekäs, R.; Laromaine, A.; Sillanpää, R.; Viñas, C.; Wade, K. *Dalton Trans.* **2004**, 3822−3828. (f) Harwell, D. E.; Mortimer, M. D.; Knobler, C. B.; Anet, F. A. L.; Hawthorne, M. F. *J. Am. Chem. Soc.* **1996**, *118*, 2679−2685. (g) Crespo, O.; Gimeno, M. C.; Laguna, A.; Ospino, I.; Aullón, G.; Oliva, J. M. *Dalton Trans.* **2009**, 3807−3813.

(4) Crespo, O.; Gimeno, M. C.; Jones, P. G.; Laguna, A. *J. Organomet. Chem.* **1997**, *531*, 87−90.

(5) (a) Wang, C.; Hang, F.; Jiang, Y.; Du, L. *J. Am. Ceram. Soc.* **2012**, *95*, 71−74. (b) Wang, C.; Huang, F.; Jiang, Y.; Li, J.; Zhou, Y.; Du, L. *Ceram. Int.* **2012**, *38*, 3081−3088. (c) Wang, C.; Jiang, Y.; Gao, Y.;

Zhou, Y.; Huang, F.; Du, L. *Polym. Eng. Sci.* **2012**, 1301−1308. (d) Díaz, C.; Abizanda, D.; Jiménez, J.; Laguna, A.; Valenzuela, M. L. *J. Inorg. Organomet. Polym. Mater.* **2006**, *16*, 211−218. (e) Armistead, J. P.; Houser, E. J.; Keller, T. M. *Appl. Organomet. Chem.* **2000**, *14*, 253−260. (f) Pehrsson, P. E.; Henderson, L. J.; Keller, T. M. *Surf. Interface Anal.* **1996**, *24*, 145−151. (g) Brown, D. A.; Colquhoun, H. M.; Daniels, J. A.; MacBride, J. A. H.; Stephenson, I. R.; Wade, K. *J. Mater. Chem.* **1992**, *2*, 793−804.

(6) Jiménez, J.; Laguna, A.; Sanz, J. A.; Díaz, C.; Valenzuela, M. L.; Jones, P. G. *Chem. Eur. J.* **2009**, *15*, 13509−135209.

(7) Díaz, C.; Valenzuela, M. L.; Laguna, A.; Lavayen, V.; Jimenez, J.; Power, L.; O'Dwyer, C. *Langmuir* **2010**, *26*, 10223−10233.

(8) Philips, D. *Photochem. Photobiol. Sci.* **2010**, *9*, 1589−1596.

(9) (a) Chen, C. H.; Shi, J. *Coord. Chem. Rev.* **1998**, *171*, 161−174. (b) Evans, R. C.; Douglas, P.; Wiscom, C. J. *Coord. Chem. Rev.* **2006**, *250*, 2093−2116. (c) Baldo, M. A.; Thompson, M. E.; Forrest, S. R. *Pure Appl. Chem.* **1999**, *71*, 2095. (d) Yersin, H. *Highly Efficient OLEDs with Phosphorescent Materials*; Wiley-VCH: Weinheim, Germany, 2008. (e) Yersin, H. *Top. Curr. Chem.* **2004**, *241*, 1−26. (f) Schwarz, G.; Reineke, S.; Rosenow, T. C.; Walter, K.; Leo, K. *Adv. Funct. Mater.* **2009**, *19*, 1319−1333. (g) Ma, X.; Zhou, X.; Shen, J.; Chao, H.-Y; Che, C.-M. *Appl. Phys. Lett.* **1999**, *74*, 1361−1363. (h) Ma, Y.; Che, C.-M.; Chao, H.-Y.; Zhou, X.; Chan, W.-H.; Shen, J. *Adv. Mater.* **1999**, *11*, 852−857.

(10) (a) Kenta, K.; Yoshiki, C. *Polym. J.* **2010**, *42*, 363−367. (b) Kenta, K.; Yuichiro, T.; Yoshiki, C. *Macromolecules* **2009**, *42*, 9238−9242. (c) Kenta, K.; Yuichiro, T.; Yoshiki, C. *Macromolecules* **2009**, *42*, 2925−2930. (d) Volvov, O. V.; L'inchik, E. A.; Volkov, V. V.; Voronina, G. S.; Yur'eva, O. P. *Russ. J. Inorg. Chem.* **1998**, *43*, 160−165. (e) Lerouge, F.; Viñas, C.; Teixidor, F.; Nuñez, R.; Abreu, A.; Xochitiotzi, E.; Santillan, R.; Farfan, N. *Dalton Trans.* **2007**, 1898−1903. (f) Ferrer-Ugalde, A.; Juárez-Pérez, E. J.; Teixidor, F.; Viñas, C.; Sillanpää, R.; Pérea-Inestrosa, E.; Núñez, R. *Chem. Eur. J.* **2012**, *18*, 544−533. (g) Lerouge, F.; Ferrer-Ugalde, A.; Viñas, C.; Teixidor, F.; Sillanpää, R.; Abren, A.; Xochitiotzi, E.; Farfán, N.; Santillán, R.; Núñez, R. *Dalton, Trans.* **2011**, *40*, 7541−7550. (h) Kunkely, H.; Vogler, A. *Inorg. Chim. Acta* **2004**, *357*, 4607−4609. (i) Juarez-Perez, E. J.; Viñas, C.; Teixidor, F.; Santillan, R.; Farfan, N.; Abreu, A.; Yepez, R.; Núñez, R. *Macromolecules* **2010**, *43*, 150−159. (j) Shin, C. H.; Han, Y.; Lee, M. H.; Do, Y. *J. Organomet. Chem.* **2009**, *649*, 1623−1631. (k) Jellis, P. A. *Comments Inorg. Chem.* **2008**, *29*, 1−25. (l) Shelkovnikov, V. V.; Ivanova, Z. M.; Orlova, N. A.; Volkov, V. V.; Drozdova, M. K.; Myakishev, K. G.; Plekhanov, A. I. *Opt. Spectrosc.* **2004**, *96*, 824−833. (m) Hong, E.; Jang, H.; Kim, Y.; Jeoung, S. C.; Do, Y. *Adv. Mater.* **2001**, *13*, 1094−1096. (n) Luguya, R.; Fronczek, F. R.; Smih, K. M.; Vicente, M. G. H. *Appl. Radiat. Isot.* **2004**, *61*, 1117−1123. (o) Zhang, D.; Dou, J.; Li, D.; Wang, D. *Inorg. Chim. Acta* **2006**, *359*, 4243−4249. (p) Ghiotti, M.; Schwab, P. F. H.; Indelli, M. T.; Chiorboli, C.; Scandola, F. *Inorg. Chem.* **2006**, *45*, 4331−4333. (q) Dou, J.; Zhang, D.; Zhu, Y.; Li, D.; Wang, D. *Inorg. Chim. Acta* **2007**, *360*, 3387−3393. (r) Weinstein, J. A.; Tierney, M. T.; Davies, E. S.; Base, K.; Robeiro, A. A.; Grinstaff, M. W. *Inorg. Chem.* **2006**, *45*, 4544−4555. (s) Crespo, O.; Gimeno, M. C.; Jones, P. G.; Laguna, A.; Lopez-de-Luzuriaga, J. M.; Monge, M.; Perez, J. L.; Ramon, M. A. *Inorg. Chem.* **2003**, *42*, 2061−2068. (t) Czerwieniec, R.; Hofbeck, T.; Crespo, O.; Laguna, A.; Gimeno, M. C.; Yersin, H. *Inorg. Chem.* **2010**, *49*, 3764−3767. (u) Crespo, O.; Díez-Gil, C.; Gimeno, M. C.; Laguna, A.; Monge, M.; Ospino, I. *Dalton Trans.* **2011**, *40*, 10038−10046. (v) Crespo, O.; Díez-Gil, C.; Gimeno, M. C.; Jones, P. G.; Laguna, A.; Tapias, J.; Ospino, I.; Villacampa, M. D.; Visbal, R. *Dalton Trans.* **2013**, *42*, 8298−8306.

(11) Usón, R.; Laguna, A.; Laguna, M. *Inorg. Synth.* **1989**, *26*, 85−91.

(12) Kivekas, R.; Sillanpáä, R.; Teixidor, F.; Vinas, C.; Nunez, R. *Acta Crystallogr., Sect.C* **1994**, *50*, 2027−2030.

(13) *SADABS (version 2.03)*; Bruker AXS, Inc., Madison, WI, 2000.

(14) Sheldrick, G. M. *SHELXL-97, Program for Crystal Structure Refinement*; University of Göttingen, Göttingen, Germany, 1977.

(15) Teixidor, F.; Viñas, C.; Abad, M. M.; Nuñez, R.; Kivekäs, R.; Sillanpää, R. *J. Organomet. Chem.* **1995**, *503*, 193. (b) Paavola, S.; Teixidor, F.; Viñas, C.; Kivekäs, R. *J. Organomet. Chem.* **2002**, *645*, 39.

(16) (a) Wiesboeck, R. A.; Hawthorne, M. F. *J. Am. Chem. Soc.* **1992**, *86*, 1642−1643. (b) Scholz, M.; Evamarie, H.-H. *Chem. Rev.* **2011**, 7035−7062.

(17) Teixidor, F.; Viñas, C.; Abad, M. M.; Kivekäs, R.; Sillanpää, R. *J. Organomet. Chem.* **1996**, *509*, 139−150.

(18) (a) Crespo, O.; Gimeno, M. C.; Laguna, A.; Jones, P. G. *J. Chem. Soc., Dalton Trans.* **1992**, 1601−1605. (b) Crespo, O.; Gimeno, M. C.; Jones, P. G.; Laguna, A. *Inorg. Chem.* **1996**, *35*, 1361−1366.

(19) Aguado, J. E.; Canales, S.; Gimeno, M. C.; Jones, P. G.; Laguna, A.; Villacampa, M. D. *Dalton Trans.* **2005**, 3005−3015.

(20) (a) Crespo, O.; Gimeno, M. C.; Laguna, A. *J. Organomet. Chem.* **2009**, *694*, 1588−1598. (b) Crespo, O.; Díez-Gil, C.; Gimeno, M. C.; Laguna, A.; Monge, M.; Ospino, I. *Dalton Trans.* **2011**, *40*, 10038−10046.

(21) (a) Biener, J.; Wittstock, A.; Zepeda-Ruiz, L. A.; Biener, M. M.; Zielasek, V.; Kramer, D.; Viswanath, R. N.; Weissmuller, J. K.; Baumer, M.; Hamza, A. V. *Nat. Mater.* **2009**, *28*, 47−51. (b) Hodge, A.; Hayes, J.; Caro, J.; Biener, J.; Hamza, A. *Adv. Eng. Mater.* **2006**, *8*, 853−857. (c) Rashid, H.; Ranjan, R.; Kotal, A.; Mandal, T. *Langmuir* **2006**, *22*, 7141−7143. (d) Shchunkin, D.; Caruso, R. *Chem. Commun.* **2003**, 1478−1479.

(22) Liu, H.; Zhang, L.; Lnag, X.; Yamaguchi, Y.; Iwasaki, H.; Inouye, Y.; Xue, Q.; Chen, M. *Sci. Rep.* **2011**, *1*, 1−5.

(23) Erlebacher, J.; Aziz, M. J.; Karma, A.; Dimitrov, N.; Sieradzki, K. *Nature* **2001**, *410*, 450−453.

(24) (a) Amarandei, G.; O'Dwyer, C.; Arshak, A.; Thiele, U.; Steiner, U.; Corcoran, D. *Langmuir* **2013**, *29*, 6706−6714. (b) Jia, X.; Listak, J.; Witherspoon, V.; Kalu, E. E.; Yang, X.; Bockstaller, M. R. *Langmuir* **2010**, *26*, 12190−12197.

(25) Paricaud, P.; Varga, S.; Jackson, G. *J. Chem. Phys.* **2003**, *118*, 8525−8536.

(26) Mackay, M. E.; Hong, Y.; Jeong, M.; Hong, S.; Russell, T. P.; Hawker, C. J.; Vestberg, R.; Douglas, J. F. *Langmuir* **2002**, *18*, 1877−1882.

(27) Wong, H. C.; Sanz, A.; Douglas, J. F.; Cabral, J. T. *J. Mol. Liq.* **2010**, *153*, 79−87.

(28) (a) Valenzuela, C. D.; Carriedo, G. A.; Valenzuela, M. L.; Zúñiga, L.; O'Dwyer, C. *Sci. Rep.* **2013**, *3*, 2642. (b) Diaz, C.; Valenzuela, M. L.; Caceres, S.; O'Dwyer, C. *J. Mater. Chem. A* **2013**, *1*, 1566−1572.